Surface Tamm states in one-dimensional photonic crystals containing anisotropic indefinite metamaterials

Yuanyuan Chen (陈园园)*, Ying Fang (房 英), Shanhong Huang (黄闪红), XiaonaYan (阎晓娜), and Jielong Shi (施解龙)

Department of Physics, Shanghai University, Shanghai 200444, China

**Corresponding author: cyyuan@staff.shu.edu.cn*

Received November 15, 2012; accepted February 25, 2013; posted online May 30, 2013

We present a theoretical study of surface Tamm states localized at an interface that separates a semi-infinite isotropic left-handed metamaterial (LHM) and one-dimensional photonic crystal made of anisotropic indefinite metamaterial (IMM) (always-cutoff material). We discuss the dispersion properties of the Tamm states in different bandgaps and demonstrate that the cap layer, angular frequency, and arrangement of photonic crystal can provide flexible control for the dispersive properties of the Tamm states.

OCIS codes: 160.3918, 240.6690, 310.4165.

doi: 10.3788/COL201311.061602.

Surface electromagnetic waves comprise a special type of localized waves that can be supported at the interface between two different physical media, where the wave vector is complex, making the wave decay exponentially away from the interface[1]. Surface waves (SWs) have been studied in periodic dielectric structures, such as photonic crystals (PCs), which can be manufactured artificially to manipulate the dispersion properties of the waves[2−6]. Staggered SWs on PCs are often called optical surface Tamm states in correlation with the nontraveling electron state on a crystal surface predicted by Tamm in 1932[7]. Such SWs supported by PCs are advantageous because the Tamm states are robust with respect to small surface roughness[8] and the low dielectric loss causes a sharp resonant coupling between the incoming light and the surface states[9].

Left-handed metamaterials (LHMs) with simultaneously negative effective dielectric permittivity and effective magnetic permeability were first suggested theoretically by Veselago in the 1960s[10]. These metamaterials have been experimentally confirmed by Smith *et al.* only a few years ago[11]. LHMs possess numerous extraordinary properties[10,12−15]. The surface states in a structure with LHM have attracted a great deal of attention[16−18]. In the presence of LHMs, the optical Tamm states can be backward, transferring energy in the direction opposite to the phase[19].

The surface states in one-dimensional (1D) PC consisting of isotropic LHM have already been investigated[19−21]. LHMs are well-known artificial materials that possess anisotropic properties because of the orientations of its arrays of spilt rings and wire in space[22,23]. One of the anisotropic metamaterials, i.e., indefinite metamaterial (IMM), in which not all the principal components of the electric permittivity and magnetic permeability tensors have the same sign, has received increasing attention over the past several years[24−26]. In this letter, we study the electromagnetic SWs guided by an interface between LHM and a 1D periodic structure consisting of anisotropic IMM layers. Based on dispersion relations[24], IMM can be identified into four classes, namely, cutoff, anti-cutoff, never-cutoff, and always-cutoff media. The 1D periodic structure in this letter contains two types of always-cutoff materials (μ_x-positive always-cutoff medium labeled as P, and μ_x-negative always-cutoff medium labeled as N for TE waves); hence, three band gaps exist. Moreover, we demonstrate that the presence of an anisotropic IMM allows the flexible control of the dispersion properties of the surface states.

In this letter, we examine the surface Tamm state at the interface between a uniform medium of isotropic LHM and a semi-infinite 1DPC made of anisotropic IMM (Fig. 1). The permittivity and permeability tensors of the anisotropic IMM have been assumed to be simultaneously diagonalized[24], i.e.,

$$\boldsymbol{\varepsilon} = \begin{pmatrix} \varepsilon_x & 0 & 0 \\ 0 & \varepsilon_y & 0 \\ 0 & 0 & \varepsilon_z \end{pmatrix}, \quad \boldsymbol{\mu} = \begin{pmatrix} \mu_x & 0 & 0 \\ 0 & \mu_y & 0 \\ 0 & 0 & \mu_z \end{pmatrix}. \quad (1)$$

Considering that 1DPC consists of one type of IMM, i.e., always-cutoff medium, the permittivity ε and permeability μ of the always-cutoff medium have the following forms[27]:

$$\varepsilon_{1y} = 1 - 144/\omega^2, \mu_{1x} = 1.2, \mu_{1z} = 1, \quad (2)$$

in the μ_x-positive always-cutoff materials P, and

$$\varepsilon_{2y} = 3, \mu_{2x} = 1 - 100/\omega^2, \mu_{2z} = 1 - 100/\omega^2, \quad (3)$$

in the μ_x-negative always-cutoff materials N, where ω is the angular frequency measured in gigahertz.

The PC is capped by a termination layer of the same material, but with selected width $d_{\mathtt{c}}$, as shown in Fig. 1. For presentation convenience, we split this termination layer P into two sublayers with lengths $d_{\mathtt{s}}$ and $d_{\mathtt{t}}$, where $(d_{\mathtt{s}} + d_{\mathtt{t}} = d_{\mathtt{c}})$. The periodic array comprise the bulk of the crystal consisting of "cells", such that each cell is made of three layers, namely, P, N, and P, with respective widths of $d_{\mathtt{t}}$,d_2, and $d_1-d_{\mathtt{t}}$[28].

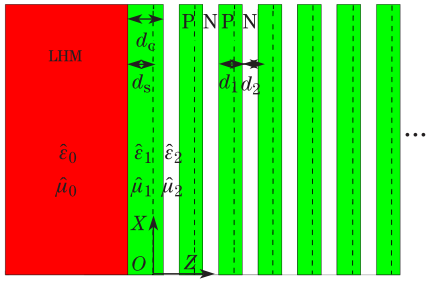

Fig. 1. (Color onlion) Sketch of a typical 1DPC consisting of alternating layers of P and N always-cutoff material. The green regions denote the P always-cutoff material. The following values are obtained:$d_1 = 16.5$ mm, $d_2 = 10$ mm, $\varepsilon_0 = -1$, and $\mu_0 = -1$.

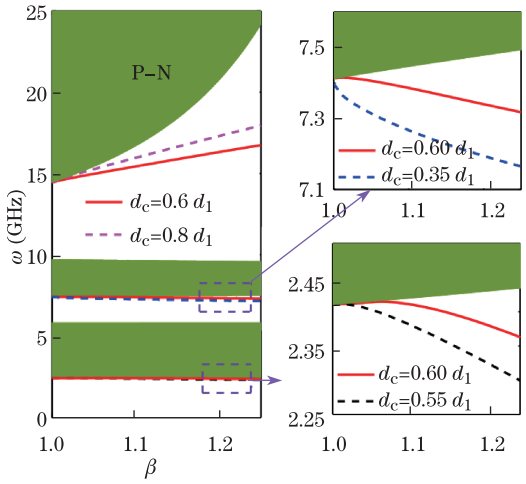

Fig. 2. (Color onlion) Dispersion diagram of the TE-polarized Tamm states in the first, second, and third bandgaps (from down to up) for the P-N periodic structures. Unshaded regions: bandgaps of 1DPC. Solid: dispersion properties of the Tamm states. Insets show the blow-up regions of the first and second bandgaps for different values of d_c.

We choose a coordinate system in which the layers have normal vectors along OZ. The electric field of the monochromatic TE-polarized waves is parallel to the OY axis. Based on Ref. [29], the electric field can be expressed as

$$\boldsymbol{E} = \boldsymbol{e}_y E(z) \exp\left[\mathrm{i}(k\beta x - \omega t)\right], \tag{4}$$

where ω is the angular frequency, $k = \omega/c$ is the vacuum wave number, β is the normalized wave number component along the interface, and c is the speed of light. $E(z)$ satisfies Maxwell equation in the form

$$\frac{\mathrm{d}^2 E(z)}{\mathrm{d}z^2} + k^2[\varepsilon(z)\mu(z) - \beta^2]E(z) = 0, \tag{5}$$

where both permittivity $\varepsilon(z)$ and permeability $\mu(z)$ characterize the transverse structure of the media. Considering the continuity conditions of the tangential components of the electric and magnetic fields at the interfaces of the periodic structure, the elements of the transfer matrix $\mathbf{M}$ are

$$\mathbf{M} = \begin{pmatrix} A & B \\ B^* & A^* \end{pmatrix}, \tag{6}$$

$$A = e^{\mathrm{i}k_1 d_1}\left[\cos k_2 d_2 + \frac{1}{2}\mathrm{i}\,(q_1 + q_2)\sin k_2 d_2\right], \tag{7}$$

$$B = e^{\mathrm{i}k_1(d_1 - 2d_\mathrm{t})}\frac{1}{2}\mathrm{i}\,(q_2 - q_1)\sin k_2 d_2, \tag{8}$$

where

$$k_j^2 = \frac{\omega^2}{c^2}\left(\varepsilon_{jy}\mu_{jx} - \frac{\mu_{jx}}{\mu_{jz}}\beta^2\right), j = 1, 2,$$
$$q_1 = \frac{k_1}{k_2}\frac{\mu_{2x}}{\mu_{1x}}, \quad q_2 = \frac{1}{k_1}.$$

The solutions of the surface Tamm states along the interface are well known, which are modes that decay from the interface in both directions, as one moves away from the surface of the PC. At the left side homogeneous medium ($z < -d\mathrm{s}$), the wave damping provides $\beta > \varepsilon_0\mu_0$. At the right-side of the periodic structure, according to Bloch's theorem, the waves follow the Bloch modes

$$E(z) = \psi(z)\exp(\mathrm{i}K_\mathrm{B}z), \tag{9}$$

where K_B is the Bloch wave number and $\psi(z)$ is the Bloch function. In the allowed bands, K_B is real. By contrast, the waves in the bandgap will decay, provided that K_B is complex. We use a well-known transfer matrix method to calculate the Bloch modes[2].

Using the continuity conditions at the interface[28], we obtain the dispersion equation of the Tamm states as

$$\frac{q_0}{k_1}\frac{\mu_{1x}}{\mu_0} = -\mathrm{i}\frac{\lambda - A - B}{\lambda - A + \widetilde{B}}, \tag{10}$$

where

$$\lambda = e^{\pm\mathrm{i}\phi} = \mathrm{Re}(A) \pm \sqrt{\mathrm{Re}(A)^2 - 1},$$
$$\widetilde{B} = e^{-2\mathrm{i}k_1 d_\mathrm{s}}B, \quad q_0 = \frac{\omega}{c}\sqrt{\beta^2 - \varepsilon_0\mu_0}.$$

The always-cutoff medium is similar to single negative materials[30]. Hence, three bandgaps exist for the periodic structure consisting of always-cutoff materials: the first gap, the first SNG gap[30]; the second gap, the zero-φ_eff gap[31]; the third gap, the Bragg gap. We present in Fig. 2 the dispersion properties of the Tamm states in the three bandgaps for different values of cap layer thickness d_c in the P-N periodic structures.

Different dispersion curves can be plotted for different values of d_c (Fig. 2), which describe the possibility of controlling the dispersion properties of the Tamm states by varying the cap layer. In addition, the bandgaps of anisotropic PC also affect the surface Tamm states. For the same values of d_c ($d_\mathrm{c} = 0.6d_1$), the dispersion curves in the three gaps are diverse. The slopes of the dispersion curves remain negative for the first and second bandgaps, whereas the dispersion curve for the third bandgap exhibits a positive slope. The slope of the dispersion curve corresponds to the group velocity of the Tamm states and

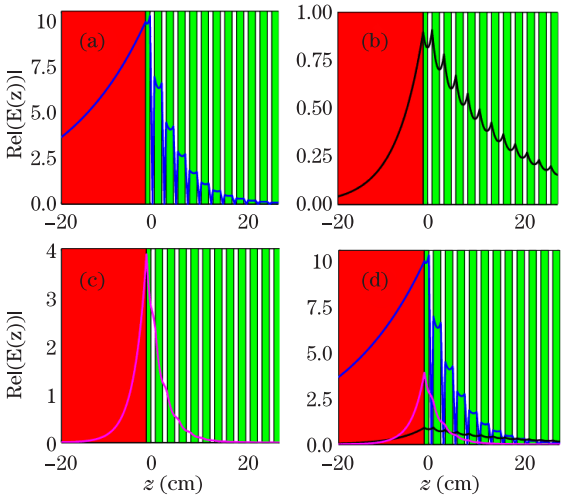

Fig. 3. (Color onlion) Backward modes of (a) the first SNG gap (ω = 2.3828 GHz) and (b) zero-φ_{eff} gap (ω = 7.3402 GHz); (c) forward mode of the third gap (ω = 16.3129 GHz); (d) amplitude distributions of the Tamm states for $d_{\mathrm{c}} = 0.6d_1$ and $\beta = 1.2$ in the three bandgaps.

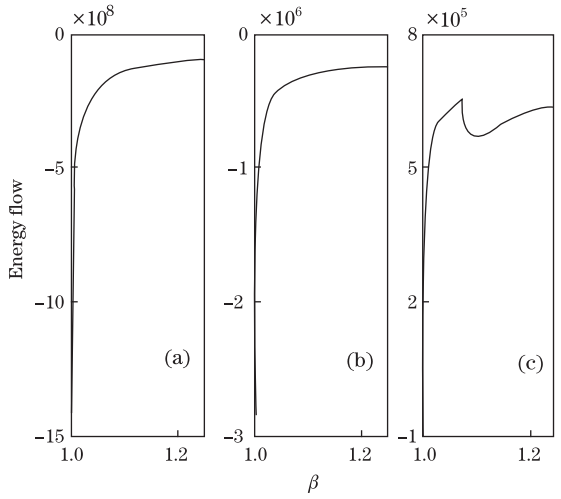

Fig. 4. Total energy flow of the Tamm states modes in the (a) first, (b) second, and (c) third bandgaps for $d_{\mathrm{c}} = 0.6d_1$.

the direction of the total energy flow. The modes with the positive (negative) slope of the dispersion curves are referred to as forward (backward) Tamm states, and the energy flow are parallel (anti-parallel) with the wave vector.

We plot the profiles of the Tamm modes with different frequencies in the three gaps in Fig. 3. For mode in Fig. 3(a), the energy flow in the LHM exceeds that in the periodic structure (slow decay of the field for $z < -d_{\mathrm{s}}$ and fast decay into the periodic structure) and the mode is backwards. Mode in Fig. 3(c) is the opposite case. We also plot the total energy flow in the modes in Fig. 4 to confirm the above discussion. The total energy flow of the modes in the first and zero-φ_{eff} bandgaps are negative, whereas that in the third bandgap remain positive. At the same time, we deduce that the energy flow of the Tamm states switch from backward to forward with an increase in frequency. Therefore, the surface Tamm states can be controlled possibly by the cap layer and the angular frequency.

Furthermore, we study the effect of the arrangement of the always-cutoff materials on the Tamm modes. In the second band gap (zero-φ_{eff} gap), we compare the dispersive curves for the different values of the cap layer d_{c} in the N-P and P-N periodic structures (with similar geometry and physical parameters) in Fig. 5. The slopes of the dispersion curves remain negative for two different structures, but with several differences. With the enhancement of d_{c}, the slopes of the dispersion curves for the N-P periodic structure increase, whereas that for the P-N periodic structure decreases slowly. This result indicates that the arrangement of the N and P layers cannot affect the energy flow direction of the Tamm states but can influence the amount of energy flow. Hence, to demonstrate this effect, we plot the total energy flow of the Tamm modes for the same frequency (ω =7.33 GHz) but different cap layers in the N-P and P-N periodic structures in Fig. 6. The corresponding modes are marked on the dispersive curves with circles and triangles in Fig. 5. Obviously, as the value of d_{c} increases, the energy flow of the surface modes increases for the N-P structure, but decreases for the P-N structure. In this letter, we only compare the energy flow value, in which

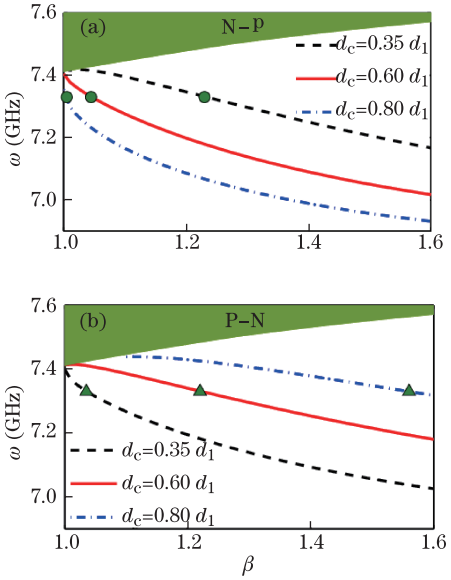

Fig. 5. (Color onlion) Dispersion diagram of the Tamm states in the second bandgap for the (a) N-P and (b) P-N periodic structures. Unshaded region: the second bandgap.

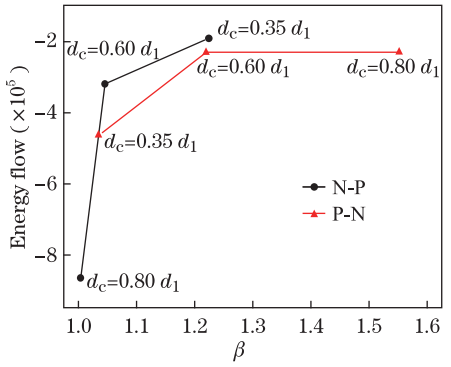

Fig. 6. (Color onlion) Total energy flow of the Tamm states with different cap layers d_{c} in the second bandgap for the N-P and P-N periodic structures.

the negative sign indicates that the total energy flow is backward.

In conclusion, we study the electromagnetic surface Tamm states supported at the interface between an isotropic LHM and a 1DPC consisting of anisotropic IMM. We discuss the properties of the surface Tamm states in the three bandgaps and demonstrate that TE-polarized SWs can be backward or forward in different bandgaps. We also show that the PC arrangement affects the amount of energy flow of the Tamm states by comparing the properties of the Tamm states with the case of N-P and P-N structure. Our results reveal that the presence of the anisotropic IMM in the PC provides more flexible control to the surface Tamm states.

This work was supported by the National Natural Sci ence Foundation of China under Grant No. 11274225.

References

1. S. Kawata, *Near-Field Optics and Surface Plasmon Polaritons* (Springer, Berlin, 2001).
2. P. Yeh, *Optical Waves in Layered Media* (Wiley, New York, 1988).
3. F. Ramos-Mendieta and P. Halevi, J. Opt. Soc. Am. B **14,** 370 (1997).
4. F. Villa, J. A. Gaspar-Armenta, and F. Ramos-Mendieta, Opt. Commun. **216,** 361 (2003).
5. A. V. Kavokin, I. A. Shelykh, and G. Malpuech, Phys. Rev. B **72,** 233102 (2005).
6. T. Goto, A. V. Dorofeenko, A. M. Merzlikin, A. V. Baryshev, A. P. Vinogradov, M. Inoue, A. A. Lisyansky, and A. B. Granovsky, Phys. Rev. Lett. **101,** 113902 (2008).
7. I. E. Tamm, Phys. Z. Sowiet **1,** 733 (1932).
8. A. P. Vinogradov, A. V. Dorofeenko, S. G. Erokhin, M. Inoue, A. A. Lisyansky, A. M. Merzlikin, and A. B. Granovsky, Phys. Rev. B **74,** 045128 (2006).
9. S. Feng, H. Sang, Z. Li, B. Cheng, and D. Zhang, J. Opt. A Pure Appl. Opt. **7,** 374 (2005).
10. V. G. Veselago, Sov. Phys. Usp. **10,** 509 (1968).
11. R. A. Shelby, D. R. Smith, and S. Schultz, Science **292,** 77 (2001).
12. J. B. Pendry, Phys. Rev. Lett. **85,** 3966 (2000).
13. I. V. Shadrivov, A. A. Zharov, and Yu. S. Kivshar, Appl. Phys. Lett. **83,** 2713 (2003).
14. Y. He, X. Zhang. Y. Yang, and C. Li, Chin. Opt. Lett. **9,** 052301 (2011).
15. M. Z. Ali, Chin. Opt. Lett. **10,** 071604 (2012).
16. R. Ruppin, Phys. Lett. A **277,** 61 (2000).
17. I. V. Shadrivov, A. A. Sukhorukov, Yu. S. Kivshar, A. A. Zharov, A. D. Boardman, and P. Egan, Phys. Rev. E **69,** 016617 (2004).
18. M. Shen, L. X. Ruan, X. Chen, J. L. Shi, H. X. Ding, N. Xi, and Q. Wang, J. Opt. **12,** 085201 (2010).
19. A. Namdar, I. V. Shadrivov, and Y. S. Kivshar, Appl. Phys. Lett. **89,** 114104 (2006).
20. A. Namdar, Opt. Commun. **278,** 194 (2007).
21. A. Namdar, S. R. Entezar, H. Rahimi, and H. Tajalli, Prog. Electromagn. Res. **13,** 149 (2010).
22. R. Marqués, F. Mesa, J. Martel, and F. Medina, IEEE Trans. Antennas Propag. **51,** 2572 (2003).
23. R. Marqués, F. Medina, and R. Rafii-El-Idrissi, Phys. Rev. B **65,** 144440 (2002).
24. D. R. Smith and D. Schurig, Phys. Rev. Lett. **90,** 077405 (2003).
25. Y. J. Xiang, X. Y. Dai, S. C. Wen, and D. Y. Fan, J. Appl. Phys. **102,** 093107 (2007).
26. W. Zhang, Y. Y. Chen, P. Hou, J. L. Shi, and Q. Wang, Phys. Rev. E **82,** 066601 (2010).
27. Y. J. Xiang, X. Y. Dai, and S. C. Wen, J. Opt. Soc. Am. B **24,** 2033 (2007).
28. J. Martorell, D. W. L. Sprung, and G. V. Morozov, J. Opt. A Pure Appl. Opt. **8,** 630 (2006).
29. G. V. Morozov, D. W. L. Sprung, and J. Martorell, Phys. Rev. E **69,** 016612 (2004).
30. L. G. Wang, H. Chen, and S. Y. Zhu, Phys. Rev. B **70,** 245102 (2004).
31. H. T. Jiang, H. Chen, H. Q. Li, Y. W. Zhang, J. Zi, and S. Y. Zhu, Phys. Rev. E **69,** 066607 (2004).